Research Square

Preprints are preliminary reports that have not undergone peer review.
They should not be considered conclusive, used to inform clinical practice,
or referenced by the media as validated information.

Chronic sleep deprivation and zinc deficiency differentially affect amyloid processing in APP/PS1 mice

Young-Hun Kim
Chung-Ang University
Byung-Sun Choi
bschoi@cau.ac.kr

Chung-Ang University

Article

Keywords: Alzheimer's disease, amyloid-β1–42, sleep deprivation, zinc deficiency, soluble amyloid, insoluble amyloid

Posted Date: March 25th, 2026

DOI: https://doi.org/10.21203/rs.3.rs-9146671/v1

License: This work is licensed under a Creative Commons Attribution 4.0 International License.
Read Full License

Additional Declarations: No competing interests reported.

Abstract

Background

Alzheimer's disease is characterized by amyloid-β plaque accumulation, which reflects an imbalance between amyloid-β production and clearance. Sleep disturbances and zinc dyshomeostasis have been associated with altered amyloid-β metabolism; however, their combined effects remain unclear. This study examined the single and combined effects of chronic sleep deprivation and dietary zinc deficiency on amyloid-β accumulation and related molecular pathways in APP/PS1 transgenic mice.

Methods

Twenty-four female APP/PS1 mice (9-month-old) were assigned to four groups (n = 6/group): control, sleep deprivation (5 h/day for 2 weeks), zinc-deficient diet (4 weeks), and combined sleep deprivation and zinc-deficient diet. Serum and brain zinc, copper, and iron concentrations were quantified using inductively coupled plasma mass spectrometry. Diethylamine-soluble and formic acid–insoluble amyloid-β1–42 levels were measured using an enzyme-linked immunosorbent assay. Brain parenchymal and endothelial-enriched fractions were used to assess proteins related to amyloid precursor protein processing and amyloid-β degradation/clearance using western blotting. Group effects and the sleep deprivation × zinc deficiency interaction were tested using two-way analysis of variance.

Results

Serum zinc concentrations decreased in the zinc-deficient diet groups, whereas brain zinc, copper, and iron concentrations remained unchanged. Soluble amyloid-β1–42 levels increased relative to the control only in the zinc-deficient diet group. Insoluble amyloid-β1–42 levels increased in all experimental groups compared to those in the control group, with the highest mean level observed in the combined exposure group. The interaction pattern did not indicate clear synergy.

Conclusions

Chronic sleep deprivation and dietary zinc deficiency differentially affect amyloid-β1–42 levels in APP/PS1 mice. These findings support the idea that sleep disturbance and micronutrient imbalance can independently influence amyloid-β production, aggregation, and clearance pathways, with combined exposure resulting in additive increases in insoluble amyloid-β burden.

Introduction

Alzheimer's disease (AD) is a progressive neurodegenerative disorder in which long preclinical phases precede overt cognitive impairment, motivating a shift from syndromic diagnosis to biologically

anchored disease [1]. Contemporary diagnostic and staging criteria explicitly center AD on in vivo biomarkers, with amyloid-β (Aβ) pathology playing a foundational role in defining the Alzheimer ’scontinuum [1, 2]. In parallel, the rapid maturation of blood-based biomarkers is accelerating clinical translation; for example, the U.S. Food and Drug Administration (FDA) recently cleared a plasma test based on the pTau217/β-amyloid 1–42 ratio to aid the detection of amyloid plaque pathology in cognitively symptomatic adults, underscoring the expanding diagnostic ecosystem surrounding Aβ biology [3]. These developments highlight the importance of mechanistic studies that explain how modifiable exposures perturb Aβ accumulation and its downstream consequences, particularly at the neurovascular interface.definitions ’ in the brain

Aβ accumulation reflects a dynamic imbalance among production, aggregation, and clearance [4]. While insoluble plaque deposition is a canonical neuropathological hallmark, a substantial body of evidence supports the view that soluble Aβ assemblies—especially oligomeric species—are potent mediators of synaptic dysfunction and cognitive impairment [5]. Accordingly, disentangling soluble versus aggregated Aβ can refine the interpretation of disease stage and mechanism beyond “total Aβ.” In preclinical brain tissue, sequential biochemical fractionation is widely used to operationalize Aβ: diethylamine (DEA) extracts soluble proteins (including soluble Aβ isoforms), whereas formic acid (FA) enables the recovery of insoluble protein aggregates, including plaque-associated Aβ [6]. This separation is particularly valuable when interrogating exposures that may differentially impact Aβ solubility/aggregation state versus net Aβ1–42 burden. In this study, we used,, and to quantify Aβ1–42 and Aβ42 levels in the human brain.

Neuroinflammation is recognized as a component of AD pathogenesis and progression, rather than merely a downstream epiphenomenon [7]. Aβ deposition can drive innate immune activation in the brain, including microglial activation of the NLRP3 inflammasome, which promotes IL-1β maturation and inflammatory amplification; genetic or pharmacologic attenuation of this axis can alter Aβ clearance and cognitive outcomes in AD models [8]. Thus, Aβ kinetics and neuroimmune signaling are tightly coupled, creating plausible routes by which lifestyle-related or nutritional perturbations shape disease trajectories. Galthe

Sleep disturbance is another modifiable risk factor. Experimental studies have demonstrated that the sleep–wake cycle regulates brain Aβ dynamics, with interstitial fluid Aβ levels correlating with wakefulness, increasing during acute sleep deprivation, and being modulated by orexin signaling; moreover, chronic sleep restriction increases plaque formation in amyloidogenic transgenic mice [9]. In humans, a single night of total sleep deprivation interferes with the physiological overnight decline in cerebrospinal fluid (CSF) Aβ42, suggesting that prolonged wakefulness can acutely shift Aβ homeostasis [10]. Additional controlled studies have reported that sleep deprivation increases overnight CSF concentrations of multiple Aβ species (Aβ38/40/42), consistent with increased production and/or impaired clearance during extended wakefulness [11]. Mechanistically, sleep has been linked to enhanced convective exchange between CSF and interstitial fluid—often discussed in the context of glymphatic transport—thereby promoting metabolite clearance, including Aβ clearance, during sleep [12].

More recent work further implicates immune pathways in the sleep–Aβ link: sleep loss worsens microglial reactivity and Aβ deposition in a TREM2-dependent manner, directly connecting sleep perturbation to microglial capacity for amyloid handling [13]. In APP/PS1 mice, chronic sleep deprivation exacerbates cognitive deficits while increasing Aβ deposition and microglial activation, highlighting a convergent neuroimmune phenotype relevant to AD [14].

Zinc is another modifiable factor that intersects with Aβ biology. Biochemical studies have shown that Zn2 + promotes Aβ precipitation/aggregation under physiologically relevant conditions, supporting a mechanistic basis for metal–amyloid interactions [15]. In vivo, zinc biology is complex and context-dependent. Notably, in APP/PS1 mice, dietary zinc deficiency paradoxically increases amyloid plaque volume, indicating that reduced dietary zinc can worsen aggregated amyloid burden under certain conditions [16]. Beyond aggregation, zinc status also intersects with innate immune signaling. In a translational study spanning human and animal data, zinc deficiency worsened cognitive decline in an AD mouse model by enhancing NLRP3-dependent inflammation, directly linking zinc status to inflammasome biology and cognitive outcomes [17]. Complementing these findings, a recent review highlights that zinc utilization by microglia can shape activation states and neuroinflammatory responses in AD, reinforcing zinc as an immunometabolic regulator within the diseased brain microenvironment [18]. Together, these observations suggest that zinc dyshomeostasis may modulate AD-like phenotypes through both amyloid-centric (aggregation/solubility) and immune-centric (inflammasome and microglial activation) mechanisms.

Sleep disturbance and micronutrient imbalance have been identified as modifiable factors associated with amyloid pathology. Experimental and clinical studies indicate that sleep deprivation can increase Aβ dynamics in the brain/CSF and exacerbate amyloid deposition, with additional evidence suggesting the involvement of immune pathways that influence amyloid handling [9, 10, 11, 12, 13, 14]. Similarly, impaired zinc homeostasis has been linked to Aβ aggregation and deposition; Zn^{2+} can promote Aβ aggregation, and dietary zinc deficiency has paradoxically been reported to increase plaque burden and exacerbate AD-like progression via inflammatory pathways in APP/PS1 mice [15, 16, 17, 18]. These findings support the notion that chronic sleep deprivation and zinc deficiency are risk-related conditions capable of disrupting Aβ homeostasis.ssthe. Although

However, most previous studies have manipulated sleep deprivation or zinc deficiency as single factors and evaluated Aβ accumulation, plaque formation, or Aβ metabolic pathways (production, clearance, and transport) in isolation. In contrast, the present study applied both single (sleep deprivation or zinc deficiency) and combined (sleep deprivation plus zinc deficiency) conditions within the same APP/PS1 female mouse model, enabling a direct comparison of their effects on soluble and insoluble Aβ1–42 and associated molecular pathways. This design reflects the frequent coexistence of sleep problems and nutritional imbalances in real-world settings and may contribute to a more realistic understanding of how modifiable risk factors shape amyloid processing. Accordingly, we investigated the single and combined effects of chronic sleep deprivation and dietary zinc deficiency on Aβ accumulation and its associated mechanisms in APP/PS1 double-transgenic mice.

Materials and Methods

Animals and Experimental Design

Twenty-four female APP/PS1 double-transgenic mice [B6.Cg-Tg(APPswe,PSEN1dE9)85Dbo/Mmjax] at a mean age of 36 weeks were obtained from the Jackson Laboratory (Bar Harbor, ME, USA) and housed in the animal center of Chung-Ang University College under standard laboratory conditions (12-h light/dark cycle, 22 ± 2℃, 50 ± 10% humidity). All experimental procedures were approved by the Institutional Animal Care and Use Committee (IACUC approval no. 202401030025) of Chung-Ang University and were conducted in accordance with the Guide for the Care and Use of Laboratory Animals.

Mice were randomly assigned to four experimental groups (n = 6 per group) based on age and body weight: control (CTL), receiving a standard AIN-93 diet and maintaining a normal sleep–wake cycle; SD, receiving a standard AIN-93 diet and subjected to chronic SD; ZD, receiving a zinc-deficient AIN-93 diet while maintaining a normal sleep–wake cycle; and SD + ZD, receiving a zinc-deficient diet and subjected to chronic SD. A zinc-deficient diet was provided for 4 weeks in the ZD and SD + ZD groups. SD was applied during the final 2 weeks in the SD and SD + ZD groups. Body weight was recorded weekly, and food intake was measured at the cage level (two cages per group).

Sleep Deprivation Protocol

Sleep Deprivation Protocol
Chronic SD was induced using an orbital shaker paradigm adapted from a previous study, which demonstrated reliable reduction of sleep without excessive physical stress. Mice in the SD and SD + ZD groups were placed in standard individual cages secured on an orbital shaker platform (Jeio Tech, Daejeon, Republic of Korea) set to 120 rpm. The shaker was programmed for intermittent movement (1 min on, 1 min off) for 5 h per day (10:00–15:00), corresponding to the light phase when the mice normally showed consolidated sleep. This protocol was followed for 14 consecutive days. This method has been validated to produce reliable SD without inducing excessive stress or pain. The control and ZD mice remained undisturbed in their home cages.

Dietary Intervention

Dietary Intervention
The diets were based on AIN-93 purified rodent formulation. The standard AIN-93 diet contained ~ 30 mg Zn/kg diet provided as zinc carbonate in the mineral mix, meeting the recommended zinc intake for rodents. The zinc-deficient diet was identical to the control diet, except that zinc carbonate was omitted from the mineral mix, resulting in < 1 mg Zn/kg diet from trace contamination. Both diets were manufactured by DooYeol Biotech (Seoul, Korea) according to AIN-93 specifications and stored at 4 ℃ until use. The control and SD groups received a standard diet, and the SD + ZD and ZD groups received a

zinc-deficient diet for 4 weeks. Food and water were provided ad libitum. Body weight and cage-level food consumption were recorded weekly to monitor general health and energy intake.

Tissue Collection and Processing

At the end of the experimental period, the mice were anesthetized using isoflurane. Blood was collected via the abdominal aorta, allowed to clot at room temperature, and centrifuged (~ 1,500 × g, 10 min) to obtain serum, which was stored at − 80°C until analysis. Brains were rapidly removed on ice. The right hemisphere was used for sequential DEA/FA Aβ extraction and ELISA. The left hemisphere was processed to separate the brain capillary endothelium (BCE; microvessel-enriched pellet) and brain parenchyma (BP; supernatant fraction) using a dextran density gradient method adapted from established protocols. Briefly, tissue was homogenized in ice-cold homogenization buffer (15 mM HEPES, 103 mM NaCl, 4.7 mM KCl, 2.5 mM $CaCl_2$, 1.2 mM KH_2PO_4, 1.2 mM $MgSO_4$, pH 7.4), mixed 1:1 with 30% (w/v) dextran (MW ~ 79,500), and centrifuged at 5,400 × g for 15 min at 4°C. The pellet was collected as the BCE fraction. The supernatant was re-centrifuged under the same conditions to obtain the BP fraction. fractions were snap-frozen in liquid nitrogen and stored at − 80°C for subsequent protein extraction.

Serum Zinc Measurement by ICP-MS

Serum zinc concentrations were measured using inductively coupled plasma mass spectrometry (ICP-MS; NexION 300S, PerkinElmer, Waltham, MA, USA), following established protocols for trace metals in biological fluids. Serum samples were diluted in 1% (v/v) ultrapure HNO_3 containing internal standards (Indium). Calibration curves were prepared using certified multi-element standards in 1% HNO_3, and quality control included procedural blanks and low/medium/high control samples. Zinc concentrations are reported as µg/L in undiluted serum.

Brain Tissue Metal Concentration Analysis

Brain metal concentrations were determined after microwave-assisted acid digestion according to a protocol based on the U.S. EPA Method 3051A. Approximately 0.5–0.8 g of whole brain tissue was placed in Teflon vessels with 8–10 mL of concentrated (70%) (v/v) $HNO_3$and subjected to microwave digestion using a CEM MARS 6 system (CEM Corp., Matthews, NC, USA). The program ramped to 175 ± 5 ℃ over ~ 5.5 min and held at that temperature for ~ 4.5 min. After cooling, the digestates were quantitatively transferred to volumetric flasks and diluted to 50 mL with 18.2 MΩ·cm deionized water. Cu, Zn, and Fe were quantified by ICP-MS with multi-element calibration (0–1000 µg/L) and indium as the internal standard. The results are expressed as µg/kg of wet tissue weight. Quality control included reagent blanks, certified reference materials, and duplicate analyses with a relative standard deviation (RSD) of < 10%.

Amyloid-β Extraction and Quantitative ELISA

Soluble and insoluble $A\beta_{1-42}$ in BP were quantified using a sequential extraction protocol followed by sandwich ELISA, as previously described, with minor modifications. Half-brains designated for Aβ measurement were homogenized in ice-cold DEA buffer (0.2% diethylamine, 50 mM NaCl) at 10% (w/v) using a Dounce tissue grinder (KIMBLE).. Homogenates were centrifuged at 30,000 × g for 1 h at 4 ℃, and the supernatant (DEA fraction) was collected as soluble Aβ. The pellet was then resuspended in 70% formic acid (FA), sonicated briefly, and centrifuged at 30,000 × g for 1 h at 4 ℃. The FA supernatant (insoluble Aβ) was neutralized by 1:20 dilution in 1 M Tris base. Both DEA and neutralized FA extracts were stored at − 80 ℃ until analysis. $A\beta_{1-42}$ concentrations were determined using a commercial ELISA kit (Human $A\beta_{1-42}$, Invitrogen #KHB3441), according to the manufacturer's instructions. Standards and samples were duplicated. $A\beta_{1-42}$ levels were expressed as pg or ng of $A\beta_{1-42}$ per mg of protein. Total $A\beta_{1-42}$ was calculated as the sum of the DEA-and FA-soluble fractions.

Protein Extraction and Western Blot Analysis

Brain parenchyma (BP) and brain capillary endothelium (BCE) fractions were homogenized in ice-cold RIPA buffer (50 mM Tris-HCl pH 7.4, 150 mM NaCl, 1% NP-40, 0.5% sodium deoxycholate, 0.1% SDS) supplemented with a protease inhibitor cocktail (Roche) and phosphatase inhibitors (Sigma-Aldrich), using a Dounce tissue grinder (Kimble). Homogenates were incubated on ice for 30 min with intermittent vortexing and centrifuged at 12,000 × g for 20 min at 4℃. Supernatants were collected, and protein concentrations were determined using the BCA Protein Assay Kit (Thermo Fisher Scientific). Equal amounts of protein (20 g) were separated on 4–12% Bis-Tris gradient gels (Bio-Rad) and transferred to PVDF membranes (Bio-Rad). Membranes were blocked with 5% BSA in TBS-T (Tris-buffered saline, 0.1% Tween-20) for 1 h at room temperature and incubated overnight at 4 ℃ with primary antibodies (see below) diluted in blocking buffer. After washing, membranes were incubated with HRP-conjugated secondary antibodies (1:5000, Cell Signaling Technology) for 1 h at room temperature. Bands were visualized using enhanced chemiluminescence (Amersham ECL, Cytiva) and imaged on an Amersham Image Quant LAS 500 system (Cytiva). Band intensities were quantified using ImageJ (NIH) and normalized to β-actin (42 kDa). Values are expressed relative to the means of the control group.

APP processing proteins in BP

Aβ production pathways, full-length APP (90–120 kDa), BACE1 (56 kDa), and ADAM10 (60/80/100 kDa) were measured in the BP. The primary antibodies used were APP (mouse monoclonal, 1:1000, Invitrogen #22C11), BACE1 (rabbit monoclonal, 1:1000, Abcam #ab108394), and ADAM10 (mouse monoclonal, 1:200, Santa Cruz #sc-48400). These markers were chosen to evaluate whether chronic SD and ZD alter β- and α-secretase-related APP processing, which, in turn, could affect $A\beta_{1-42}$ generation.

Aβ degrading enzymes (IDE, NEP) and AQP4 in BP

Levels of amyloid-β (Aβ)-degrading enzymes were assessed using western blotting. Insulin-degrading enzyme (IDE, 118 kDa), neprilysin (NEP, 100 kDa), and aquaporin-4 (AQP4, 32 kDa) levels were measured in BP extracts. The primary antibodies used were anti-IDE (rabbit monoclonal, 1:1000, Abcam #ab32216), anti-NEP (rabbit polyclonal, 1:200, Santa Cruz #SC-194), and AQP4 (rabbit polyclonal, 1:200, Bosterbio #PA1937). IDE, NEP, and AQP4 are key enzymes that degrade Aβ in the brain parenchyma.

BBB Aβ transporters and tight junction protein in BCE

BBB transport-related proteins and barrier integrity markers were examined in BCE fractions, including P-gp/ABCB1 (~ 170 kDa), LRP1 (~ 85 kDa), RAGE (~ 50 kDa), and tight-junction protein claudin-5 (~ 22 kDa). Primary antibodies used were P-gp (rabbit monoclonal, Abcam #ab170904), LRP1 (rabbit polyclonal, Abcam #ab92544), RAGE (rabbit polyclonal, Abcam #ab3611), and claudin-5 (rabbit monoclonal, Abcam #ab131259). Protein bands were visualized with enhanced chemiluminescence and quantified by densitometry.

Statistical Analysis

All statistical analyses were performed using GraphPad Prism software (version 10; GraphPad Software, San Diego, CA, USA). Data are presented as the mean ± standard deviation unless otherwise specified. Normality of distributions was assessed using the Shapiro–Wilk test. For normally distributed data, one-way analysis of variance (ANOVA) was used to compare the four groups (CTL, SD, ZD, and SD + ZD). When ANOVA indicated a significant group effect ($p < 0.05$), Tukey's honest significant difference (HSD) post hoc test was applied for pairwise comparisons. For non-normally distributed data, the Kruskal–Wallis test followed by Dunn's multiple comparison test was used. A two-sided p value < 0.05 was considered statistically significant. ($^{*}p < 0.05$, $^{**}p < 0.01$, $^{***}p < 0.001$)

Results

Body weight and food consumption

Body weight was monitored weekly during the 4-week intervention period. The final body weights did not differ significantly among the four groups (control, SD, ZD, and SD + ZD; ANOVA, $p = 0.57$). The mean (± SD) endpoint body weights were 26.0 ± 2.9 g in the control group, 24.2 ± 4.0 g in the SD group, 24.8 ± 1.9 g in the ZD group, and 26.3 ± 3.1 g in the SD + ZD group ($n = 6$ per group), indicating that neither chronic SD nor ZD, alone or in combination, produced overt changes in overall body mass (Fig. 1A, 1B).

Weekly food consumption was recorded per cage (g/week per cage; $n = 2$ cages per group). Across the 4-week intervention, food intake appeared broadly comparable between groups (Fig. 1B). Because intake was measured at the cage level, these data are presented descriptively and were not subjected to inferential statistics at the individual level.

Serum Zinc Concentration by ICP-MS

Serum zinc concentration was strongly affected by dietary intervention (Fig. 2; Table 1). In one-way ANOVA across the four groups, overall group differences were significant ($p < 0.001$), and Tukey's post hoc test indicated that serum zinc did not differ between the control and SD mice, whereas both ZD and SD + ZD groups showed markedly reduced serum zinc levels relative to the control. Because the design was factorial (SD ± and ZD ±), we additionally estimated main effects and interactions using pre-specified contrasts (Table S1). The ZD main effect indicated a large reduction in serum zinc levels ($p < 0.001$). The SD main effect was smaller and did not reach significance at two-sided ($p = 0.98$). The SD×ZD interaction contrast was significant ($p < 0.05$), suggesting that the SD protocol further exacerbated systemic zinc depletion in the setting of dietary zinc deficiency.

Table 1
Serum zinc level (Mean ± SD; μg/L)

Group	N	Mean	SD	P value
Control	6	765.89	149.86	
Sleep deprivation	6	784.39	47.84	= 0.9835
Zinc deficiency	6	467.6	61.52	< 0.0001
Sleep deprivation + Zinc deficiency	6	293.9	55.00	< 0.0001
Serum zinc concentration values across groups. Includes mean ± SD.				

Brain Tissue Metal Concentrations

Brain Cu, Zn, and Fe concentrations were quantified by ICP-MS after acid digestion (Table 2; Fig. 3). One-way ANOVA did not indicate significant group differences for Cu ($p = 0.509$), Zn ($p = 0.404$), or Fe ($p = 0.213$). Consistent with these results, factorial contrast estimates showed no significant SD main effect, ZD main effect, or SD×ZD interaction for any metal (all $p > 0.12$; Table 2), supporting the interpretation that dietary Zn deficiency induced systemic depletion without detectable changes in bulk whole-brain metal concentrations under the present conditions.

Table 2
Brain Cu, Zn, Fe data summary.

Metal	Control	Sleep deprivation	Zinc deficiency	Sleep deprivation + Zinc deficiency	p-value
Copper	174.9 ± 50.4	137.5 ± 52.0	154.0 ± 48.3	187.0 ± 82.9	0.509
Zinc	443.8 ± 124.9	342.4 ± 136.1	419.8 ± 142.7	507.9 ± 235.2	0.404
Iron	608.9 ± 187.2	422.9 ± 156.4	673.4 ± 230.8	650.7 ± 283.4	0.213
Summary statistics of brain metal content (Cu, Zn, and Fe) based on one-way analysis of variance and post-hoc comparisons.					

Brain $A\beta_{1-42}$ levels (DEA-soluble, FA-insoluble, total)

Aβ1–42 levels were quantified in the DEA-soluble, FA-insoluble, and combined (DEA + FA) fractions by ELISA (Fig. 4; Table 3). For the DEA-soluble fraction, one-way ANOVA showed an overall group effect ($p < 0.05$), and Tukey's post hoc test indicated a significant increase in the ZD group versus the control, whereas the SD and SD + ZD groups were not significantly different from the control. In factorial contrast analysis, the ZD main effect on DEA-soluble Aβ1–42 was significant ($p < 0.05$), whereas the SD main effect and SD×ZD interaction were not significant (Table 3), supporting the interpretation that dietary zinc deficiency preferentially increased the soluble Aβ1–42 pool under the present conditions.

Table 3
Comprehensive Summary of Soluble (DEA), Insoluble (FA), Total Aβ1–42, and Aggregation Index.

Group	N	DEA (pg/mg)	FA (pg/mg)	Total (pg/mg)	FA/DEA Ratio
Control	6	9.12 ± 0.96	20.05 ± 0.66	29.18 ± 1.49	2.21 ± 0.18
Sleep deprivation	6	9.61 ± 0.87	**31.55 ± 1.09	*41.16 ± 1.06	3.31 ± 0.33
Zinc deficiency	6	*12.15 ± 0.92	*28.33 ± 0.73	*40.48 ± 1.19	2.34 ± 0.16
Sleep deprivation + Zinc deficiency	6	11.62 ± 3.35	***34.58 ± 9.30	**46.20 ± 12.64	2.99 ± 0.07
Data are presented as mean ± SD. ($^{*}p < 0.05$, $^{**}p < 0.01$, $^{***}p < 0.001$ vs Control)					

FA-insoluble $A\beta_{1-42}$, reflecting more aggregated species, was more robustly affected (ANOVA, $p < 0.01$). All three intervention groups (SD, $p < 0.01$; ZD, $p < 0.05$; and SD + ZD, $P < 0.01$) exhibited significantly elevated FA-insoluble $A\beta_{1-42}$ compared to control. No significant differences were observed among the three intervention groups (Fig. 4B, Table 3).

Total $A\beta_{1-42}$ (DEA + FA) levels also differed significantly among groups (ANOVA, $p < 0.01$). Compared with control mice, which showed the lowest total $A\beta_{1-42}$ levels, all intervention groups (SD, ZD, and SD + ZD) had significantly higher total $A\beta_{1-42}$ levels ($p < 0.05$); SD + ZD is the highest increase ($p < 0.01$), with no significant pairwise differences among the three treated groups (Fig. 4C, Table 3).

$A\beta_{1-42}$ expression (~ 46, ~ 90 kDa) in brain parenchyma

$A\beta_{1-42}$ immunoreactivity in the brain parenchyma was also assessed by western blotting, which revealed prominent bands at approximately ~ 46 and ~ 90 kDa (Fig. 5). Because these apparent molecular weights do not correspond directly to canonical Aβ monomer or small oligomer sizes, we report these signals operationally by apparent molecular weight and interpret them cautiously. The ~ 46 kDa band did not differ among groups (one-way ANOVA, $p = 0.911$), whereas the ~ 90 kDa band was increased in the

SD group compared to the control ($p < 0.05$), consistent with the preferential accumulation of higher-molecular-weight Aβ-immunoreactive species under the SD protocol.

Aβ production and processing proteins (APP, ADAM10, BACE1) in brain parenchyma

To determine whether changes in $A\beta_{1-42}$ levels were associated with altered APP processing, APP, BACE1, and ADAM10 expression in the brain parenchyma was examined using western blotting (Fig. 6). APP (90–120 kDa) levels did not differ significantly among the groups (one-way ANOVA, n.s.), indicating that the overall APP abundance was unchanged (Fig. 6A). The α-secretase ADAM10 (60/80/100 kDa) exhibited a significant group effect. ADAM10 expression was numerically increased compared with that in the control, and Tukey's post hoc test demonstrated a significant elevation in the ZD group compared with that in the control ($p < 0.05$), whereas the increases in the SD and SD + ZD groups did not reach statistical significance (Fig. 6B).

BACE1 (56 kDa) levels were significantly increased in the SD group. Post hoc analysis (Tukey's test) revealed that BACE1 expression was significantly higher in SD mice than in control mice ($p < 0.05$); however, there were no significant differences among the ZD and SD + ZD groups. These data indicate selective upregulation of β-secretase expression under chronic SD (Fig. 6C). Chronic SD enhances β-secretase (BACE1) expression, whereas ZD preferentially upregulates α-secretase ADAM10 without major changes in total APP levels.

Aβ-degrading enzymes NEP, IDE and AQP4 in brain parenchyma

In the brain parenchyma, the Aβ-degrading enzymes IDE (~ 118 kDa) and NEP (~ 100 kDa) were quantified by western blotting and showed no significant differences among the groups (Fig. 7A,B). AQP4 (~ 35 kDa), a perivascular water channel implicated in glymphatic exchange, was also quantified in BP fractions and did not differ among the groups (Fig. 7C).

Aβ transporters and tight junction protein in brain capillary endothelium and brain parenchyma

BBB-associated proteins were examined in BCE fractions, including P-gp/ABCB1 (~ 170 kDa), LRP1 (~ 85 kDa), RAGE (~ 50 kDa), and claudin-5 (~ 22 kDa) (Fig. 8). No significant group differences were detected for these BCE proteins. These abundance-level findings do not exclude functional or localization changes in transport or perivascular clearance pathways.

Discussion

Alzheimer's disease (AD) is characterized by its core pathologies—amyloid-β (Aβ) plaques and tau neurofibrillary tangles—and the field has increasingly moved toward biomarker-driven frameworks and

earlier detection strategies that emphasize amyloid biology as a foundational component of the AD continuum. In parallel, decades of therapeutic efforts targeting Aβ production and aggregation have faced substantial translational barriers. In particular, β- and γ-secretase inhibitor programs have been limited by adverse effects, cognitive worsening, or futility, as illustrated by multiple phase 3 trials of BACE and γ-secretase inhibitors (e.g., verubecestat, atabecestat, semagacestat, and avagacestat) [19, 20, 21, 22, 23]. More recently, anti-amyloid monoclonal antibodies have demonstrated modest clinical slowing in early symptomatic AD but remain constrained by implementation complexity and safety concerns, such as amyloid-related imaging abnormalities (ARIA) [24, 25, 26]. Against this backdrop, identifying modifiable factors that perturb Aβ homeostasisand clarifying the mechanisms by which they act remains important for prevention-oriented strategies and mechanistic risk modeling, consistent with contemporary dementia risk-reduction guidance [27, 28].

In this study, we tested two modifiable exposures—chronic sleep deprivation (SD) and dietary zinc deficiency (ZD)— individually and in combination in APP/PS1 mice, with particular emphasis on separating soluble versus insoluble Aβ pools. A key observation was that Aβ1–42 responses differed by fraction and exposure: ZD selectively increased the DEA-soluble pool, whereas all intervention groups increased FA-insoluble Aβ1–42, with the combined SD + ZD group showing the highest mean insoluble burden but without evidence of a strong interaction beyond additivity. This fraction-resolved pattern supports the interpretation that SD and ZD reshape amyloid biology through partially distinct upstream pressures that converge on aggregated Aβ accumulation.

The SD phenotype aligns with a shift toward amyloidogenic processing. Sleep–wake regulation of Aβ kinetics is supported by both animal and human evidence, including orexin-linked modulation of Aβ dynamics and increased Aβ during extended wakefulness or sleep loss [9, 10, 11]. Sleep has also been linked to brain-wide metabolite clearance processes (often discussed as glymphatic exchange), providing a mechanistic rationale for why sustained sleep loss can bias the balance between Aβ production and clearance [12]. In animal models, sleep deprivation has been shown to exacerbate Aβ deposition and microglial reactivity in a TREM2-dependent manner, supporting a neuroimmune–amyloid coupling framework for sleep-related amyloid accumulation [13]. Consistent with these concepts, our molecular data indicate that SD selectively increased BACE1, the β-secretase that initiates amyloidogenic APP processing, a recognized control point for cerebral Aβ generation [19]. Together, these findings support a model in which chronic SD increases the propensity for amyloidogenic processing and promotes the accumulation of higher-order Aβ assemblies, consistent with experimental evidence that sleep loss can accelerate amyloid deposition and worsen disease-relevant phenotypes in amyloid models [14, 29].

ZD produced a distinct pattern, including a selective increase in DEA-soluble Aβ1–42 and preferential upregulation of ADAM10. Zinc is deeply intertwined with amyloid biology and neuroimmune function. Zn^{2+} can promote Aβ aggregation under physiologically relevant conditions [15], and in APP/PS1 mice, dietary zinc deficiency has paradoxically been reported to increase plaque burden, indicating that systemic deficiency does not necessarily reduce aggregated amyloid in vivo and may worsen it under

certain conditions [16]. Zinc status also intersects with innate immune pathways relevant to AD progression, including NLRP3-dependent mechanisms [17], and microglial zinc utilization has been highlighted as an immunometabolic regulator in AD-relevant contexts [18]. Human observational data further support translational relevance, reporting associations between lower serum zinc and higher in vivo brain amyloid deposition [30]. Although ADAM10 is the physiologically relevant constitutive α-secretase of APP and is generally viewed as supporting non-amyloidogenic processing [31], increased ADAM10 abundance does not necessarily imply reduced Aβ generation, because APP processing reflects integrated regulation of secretase activity, substrate availability, trafficking, and competing pathways. Therefore, the coexistence of elevated ADAM10 with increased soluble and insoluble Aβ1–42 suggests that ZD-driven amyloid effects may be mediated less by a simple α/β secretase "switch" and more by zinc-sensitive changes in local aggregation chemistry, compartmental homeostasis, or immune-linked amyloid handling [15, 16, 17, 18].

A central goal of this factorial design was to evaluate whether combined SD + ZD produces synergy. Instead, combined exposure yielded a pattern consistent with the additive accumulation of insoluble Aβ1–42. Several interpretations are plausible. First, SD and ZD may act through separable mechanisms —SD biasing amyloidogenic processing (BACE1) and higher-order assembly, and ZD altering soluble pool dynamics and zinc-dependent microenvironmental factors—such that the effects sum rather than multiply over the tested window. Second, interaction effects may be difficult to resolve with a modest sample size and short exposures, particularly in a transgenic model that already exhibits substantial amyloid pathology. Third, the non-overlapping duration of exposures (ZD for 4 weeks; SD for the final 2 weeks) may favor additive rather than synergistic emergence. Importantly, to our knowledge, prior work has largely manipulated sleep loss or zinc dyshomeostasis as single factors in AD models, whereas a direct within-model comparison of single versus combined SD and ZD is not well represented in the literature. Thus, the present study adds value by testing a co-exposure scenario that better approximates real-world clustering of lifestyle and nutritional stressors and by showing that combined exposure can increase aggregated amyloid burden without necessarily producing a multiplicative interaction effect.

Implications

These findings support the concept that modifiable exposures can differentially bias soluble versus insoluble Aβ pools and may, therefore, influence distinct stages or modes of amyloid pathology. In the context of evolving biomarker paradigms and modestly effective but resource-intensive anti-amyloid therapeutics [24, 25, 26], clarifying which common modifiable factors shift Aβ production, assembly, and compartmentalization may help refine prevention strategies and mechanistic risk modeling aligned with contemporary public health guidance [27, 28]. More broadly, the observation that SD and ZD converge on increased insoluble Aβ while diverging in soluble effects is consistent with a systems view of AD in which multiple upstream perturbations converge on shared downstream phenotypes through partially separable mechanistic routes [32, 33].

Limitations

This study has several limitations. First, only female APP/PS1 mice were evaluated; sex-dependent differences in sleep physiology, micronutrient metabolism, and amyloid progression may influence generalizability. Second, we did not include behavioral testing or direct neuroinflammatory readouts (e.g., microglial/astrocytic activation markers, cytokines, and inflammasome components), limiting inferences about cognitive relevance and immune-mediated mechanisms. Third, key clearance-related pathways were assessed primarily at the level of protein abundance by western blotting; functional changes in enzyme activity (e.g., IDE/NEP), transporter activity/localization (e.g., LRP1/ABCB1/RAGE), or perivascular AQP4 polarization and glymphatic flux could occur without detectable changes in total protein levels. Finally, Aβ was quantified as Aβ1–42 in soluble (DEA) and insoluble (FA) fractions; additional species (e.g., Aβ1–40, Aβ38) and post-translationally modified forms were not assessed and could further refine mechanistic interpretations.

Future studies should include both sexes, incorporate cognitive and neuroimmune endpoints, quantify secretase and Aβ-degrading enzyme activity, and assess neurovascular/glymphatic function with spatially resolved measures (e.g., immunohistochemistry for plaque load and AQP4 polarization, BBB permeability assays, or tracer-based clearance paradigms).

Conclusions

Chronic sleep deprivation and dietary zinc deficiency differentially affected Aβ1–42 pools in female APP/PS1 mice. Zinc deficiency selectively increased DEA-soluble Aβ1–42, whereas both exposures increased FA-insoluble Aβ1–42, with the combined condition showing the highest mean insoluble burden but without clear evidence of a synergistic interaction beyond an additive pattern. At the molecular level, sleep deprivation and zinc deficiency showed distinct signatures in APP-processing proteins (BACE1 versus ADAM10), supporting partially separable mechanistic routes converging on increased aggregated amyloid. These findings highlight the importance of considering co-occurring lifestyle and nutritional stressors when interpreting amyloid processing and suggest that improving sleep and micronutrient status may represent complementary, modifiable targets for strategies aimed at mitigating amyloid burden.

Declarations

Funding Statement: Not applicable

Ethical Compliance: All experimental procedures were approved by the Institutional Animal Care and Use Committee (IACUC approval no. 202401030025) and conducted in accordance with the Guide for the Care and Use of Laboratory Animals and relevant institutional guidelines.

Data Access Statement: The datasets generated and/or analyzed during the current study are available from the corresponding author on reasonable request.

Conflict of Interest declaration: The authors declare that they have no competing interests.

Author Contributions: [YHK] conceived and designed the study. [YHK] performed the animal experiments and sample collection. [YHK] conducted the ICP-MS analyses. [YHK] performed biochemical fractionation, ELISA, and western blotting. [YHK] analyzed the data and drafted the manuscript. [BSC] supervised the study and critically revised the manuscript. All authors read and approved the final manuscript.

References

1. Jack, C. R. Jr et al. NIA-AA Research Framework: Toward a biological definition of Alzheimer's disease. *Alzheimers Dement.* **14** (4), 535–562 (2018).
2. Jack, C. R. Jr et al. Revised criteria for diagnosis and staging of Alzheimer's disease: Alzheimer's Association Workgroup. *Alzheimers Dement.* **20** (8), 5143–5169. 10.1002/alz.13859 (2024).
3. US Food and Drug Administration. FDA clears first blood test used in diagnosing Alzheimer's disease. (2025).
4. Hampel, H. et al. The amyloid-β pathway in Alzheimer's disease. *Mol. Psychiatry.* **26**, 5481–5503. 10.1038/s41380-021-01249-0 (2021).
5. Selkoe, D. J. Soluble oligomers of the amyloid β-protein impair synaptic plasticity and behavior. *Behav. Brain Res.* **192** (1), 106–113. 10.1016/j.bbr.2008.02.016 (2008).
6. Casali, B. T. & Gary, E. Landreth. Aβ extraction from murine brain homogenates. *Bio-protocol* 6.8 : e1787-e1787. (2016). 10.21769/BioProtoc.1787
7. Heneka, M. T. et al. Neuroinflammation in Alzheimer's disease. *Lancet Neurol.* **14** (4), 388–405. 10.1016/S1474-4422(15)70016-5 (2015).
8. Heneka, M. T. et al. NLRP3 is activated in Alzheimer's disease and contributes to pathology in APP/PS1 mice. *Nature* **493** (7434), 674–678. 10.1038/nature11729 (2013).
9. Kang, J. E. et al. Amyloid-β dynamics are regulated by orexin and the sleep-wake cycle. *Science* **326** (5955), 1005–1007. 10.1126/science.1180962 (2009).
10. Ooms, S. et al. Effect of 1 night of total sleep deprivation on cerebrospinal fluid β-amyloid 42 in healthy middle-aged men: a randomized clinical trial. *JAMA Neurol.* **71** (8), 971–977. 10.1001/jamaneurol.2014.1173 (2014).
11. Lucey, B. P. et al. Effect of sleep on overnight cerebrospinal fluid amyloid β kinetics. *Ann. Neurol.* **83** (1), 197–204. 10.1002/ana.25117 (2018).
12. Xie, L. et al. Sleep drives metabolite clearance from the adult brain. *Science* **342** (6156), 373–377. 10.1126/science.1241224 (2013).
13. Parhizkar, S. et al. Sleep deprivation exacerbates microglial reactivity and Aβ deposition in a TREM2-dependent manner in mice. *Sci. Transl Med.* **15**, eade6285. 10.1126/scitranslmed.ade6285 (2023).
14. Wang, C. et al. Chronic sleep deprivation exacerbates cognitive and synaptic plasticity impairments in APP/PS1 transgenic mice. *Behav. Brain Res.* **412**, 113400. 10.1016/j.bbr.2021.113400 (2021).

15. Huang, X. et al. Zinc-induced Alzheimer's Aβ1–40 aggregation is mediated by conformational factors. *J. Biol. Chem.* **272** (42), 26464–26470. 10.1074/jbc.272.42.26464 (1997).
16. Stoltenberg, M. et al. Amyloid plaques arise from zinc-enriched cortical layers in APP/PS1 transgenic mice and are paradoxically enlarged with dietary zinc deficiency. *Neuroscience* **150** (2), 357–369. 10.1016/j.neuroscience.2007.09.014 (2007).
17. Rivers-Auty, J. et al. Zinc status alters Alzheimer's disease progression through NLRP3-dependent inflammation. *J. Neurosci.* **41** (13), 3025–3038. 10.1523/JNEUROSCI.1980-20.2020 (2021).
18. Shippy, D. C., Oliai, S. F. & Ulland, T. K. Zinc utilization by microglia in Alzheimer's disease. *J. Biol. Chem.* **300** (5), 107306. 10.1016/j.jbc.2024.107306 (2024).
19. Yan, R. & Vassar, R. Targeting the β secretase BACE1 for Alzheimer's disease therapy. *Lancet Neurol.* **13** (3), 319–329. 10.1016/S1474-4422(13)70276-X (2014).
20. Egan, M. F. et al. Randomized trial of verubecestat for mild-to-moderate Alzheimer's disease. *N Engl. J. Med.* **378** (18), 1691–1703. 10.1056/NEJMoa1706441 (2018).
21. Sperling, R., Henley, D., Aisen, P. S., Raman, R., Donohue, M. C., Ernstrom, K., …Romano, G. (2021). Findings of efficacy, safety, and biomarker outcomes of atabecestat in preclinical Alzheimer disease: a truncated randomized phase 2b/3 clinical trial.JAMA neurology, 78(3), 293–301.doi:10.1001/jamaneurol.2020.4857..
22. Doody, R. S. et al. A phase 3 trial of semagacestat for treatment of Alzheimer's disease. *N Engl. J. Med.* **369** (4), 341–350. 10.1056/NEJMoa1210951 (2013).
23. Coric, V. et al. Safety and tolerability of the γ-secretase inhibitor avagacestat in a phase 2 study of mild to moderate Alzheimer disease. *Arch. Neurol.* **69** (11), 1430–1440. 10.1001/archneurol.2012.2194 (2012).
24. van Dyck, C. H. et al. Lecanemab in early Alzheimer's disease. *N Engl. J. Med.* **388** (1), 9–21. 10.1056/NEJMoa2212948 (2023).
25. Sims, J. R. et al. Donanemab in early symptomatic Alzheimer disease: the TRAILBLAZER-ALZ 2 randomized clinical trial. *JAMA* **330** (6), 512–527. 10.1001/jama.2023.13239 (2023).
26. Salloway, S. et al. Amyloid-related imaging abnormalities in 2 phase 3 studies evaluating aducanumab in patients with early Alzheimer disease. *JAMA Neurol.* **79** (1), 13–21. 10.1001/jamaneurol.2021.4161 (2022).
27. Livingston, G. et al. Dementia prevention, intervention, and care: 2024 report of the Lancet standing Commission. *Lancet* **404** (10452), 572–628. 10.1016/S0140-6736(24)01296-0 (2024).
28. World Health Organization. *Risk reduction of cognitive decline and dementia: WHO guidelines* (World Health Organization, 2019).
29. Minakawa, E. N. et al. Chronic sleep fragmentation exacerbates amyloid β deposition in Alzheimer's disease model mice. *Neurosci. Lett.* **653**, 362–369. 10.1016/j.neulet.2017.05.054 (2017).
30. Kim, J. W. et al. Serum zinc levels and in vivo beta-amyloid deposition in the human brain. *Alzheimers Res. Ther.* **13**, 190. 10.1186/s13195-021-00931-3 (2021).

31. Kuhn, P. H. et al. ADAM10 is the physiologically relevant, constitutive α-secretase of the amyloid precursor protein in primary neurons. *EMBO J.* **29** (17), 3020–3032. 10.1038/emboj.2010.167 (2010).
32. De Strooper, B. & Karran, E. The cellular phase of Alzheimer's disease. *Cell* **164** (4), 603–615. 10.1016/j.cell.2015.12.056 (2016).
33. Scheltens, P. et al. Alzheimer's disease. *Lancet* **397** (10284), 1577–1590. 10.1016/S0140-6736(20)32205-4 (2021).

Figures

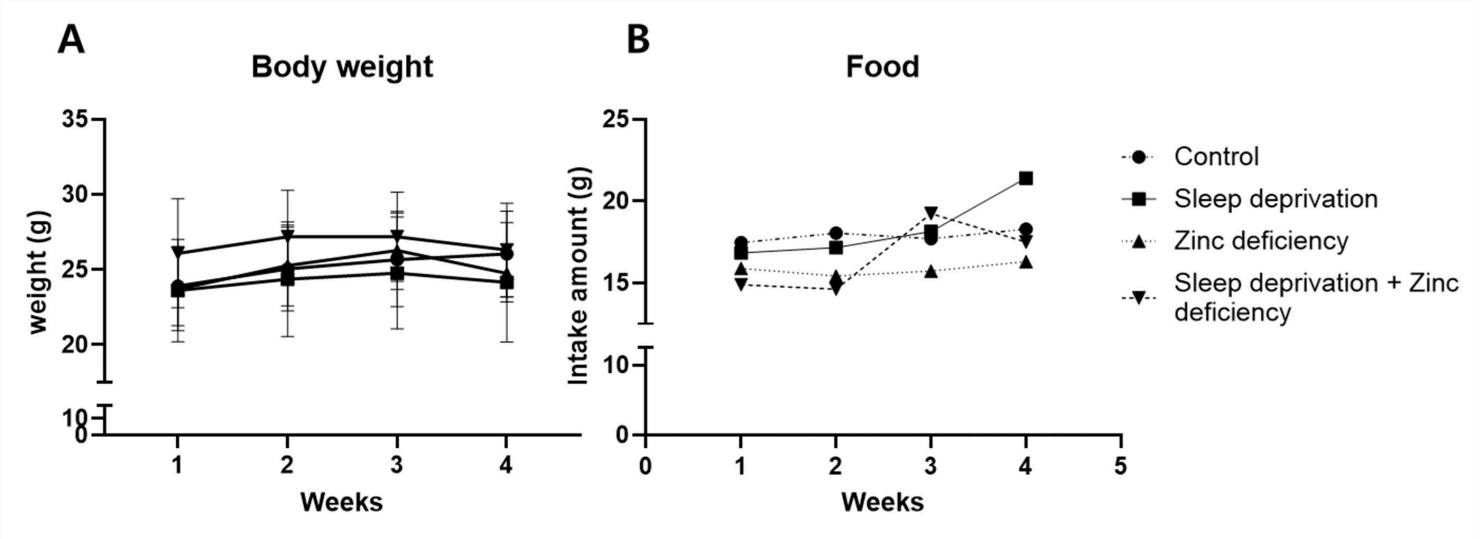


Figure 1

Body Weight Changes and Food Intake 4-Week Experimental Period. body weights and food intake across four experimental groups (n = 6 per group for body weight; n = 2 cages per group for food). Data are shown as mean ± SD.

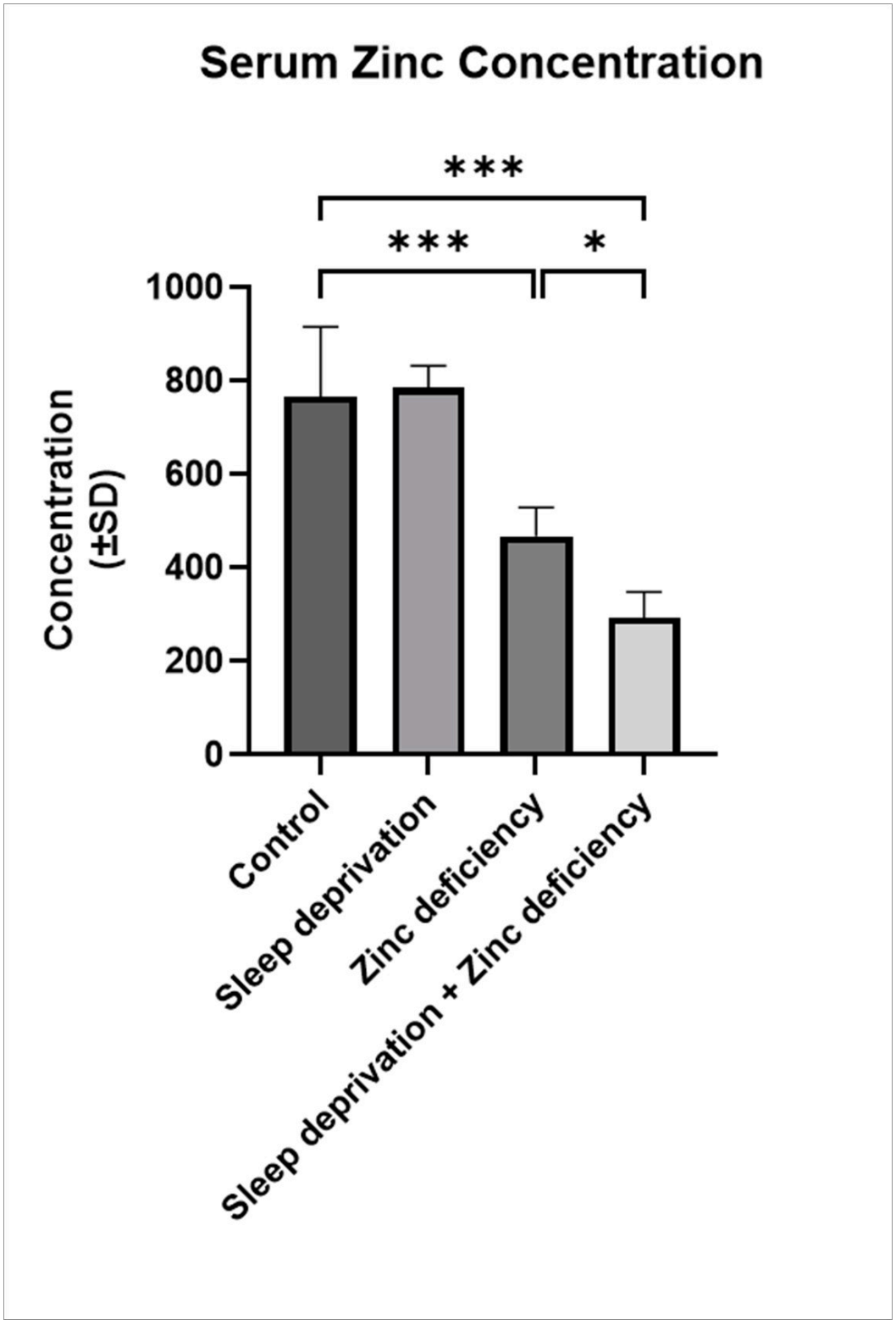


Figure 2

Serum zinc concentrations (ICP-MS). Serum zinc concentrations measured by ICP-MS after dietary and sleep interventions. Data are presented as mean±SD (n= 6 per group) ($^{*}p < 0.05$, $^{**}p < 0.01$, $^{***}p < 0.001$).

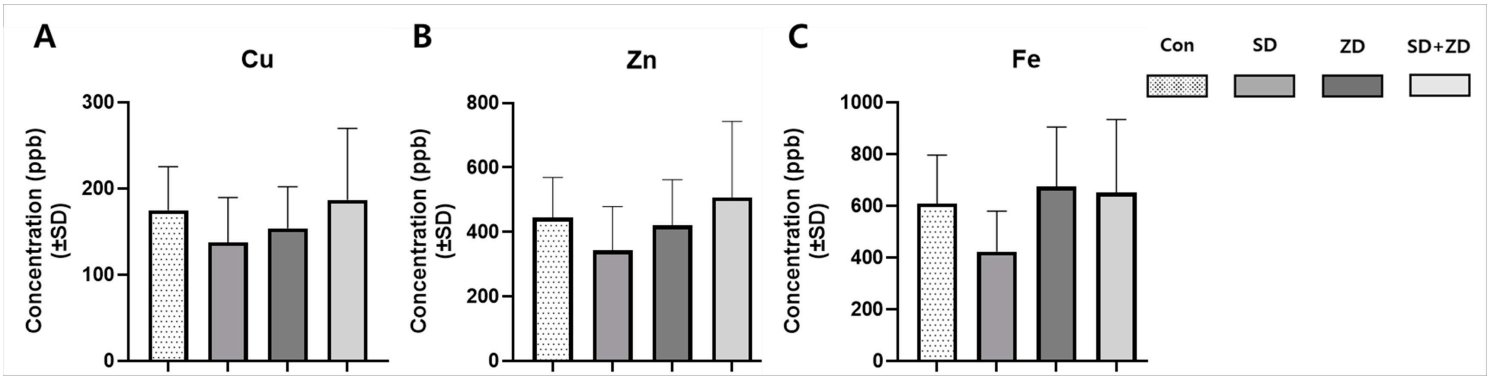


Figure 3

Brain metal concentrations (Cu, Zn, Fe) by ICP-MS. Copper, zinc, and iron concentrations in whole brain homogenates measured by ICP-MS. Values represent mean±SD (n = 6 per group). (*p <0.05, **p <0.01, ***p <0.001).

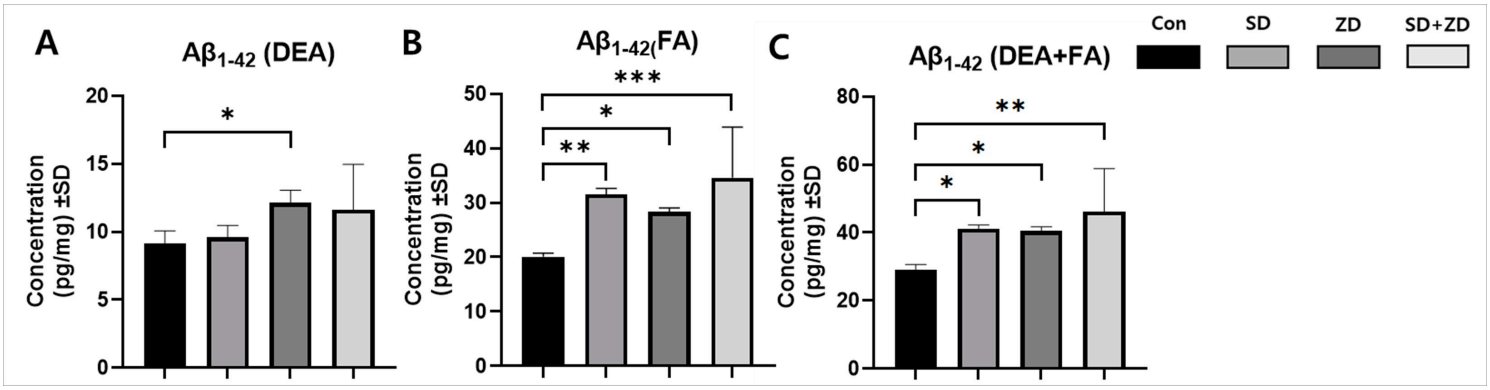


Figure 4

DEA buffer and FA buffer Aβ $_{1\text{-}42}$ concentration. Values represent mean±SD (n = 6 per group). (*p <0.05, **p <0.01, ***p <0.001).

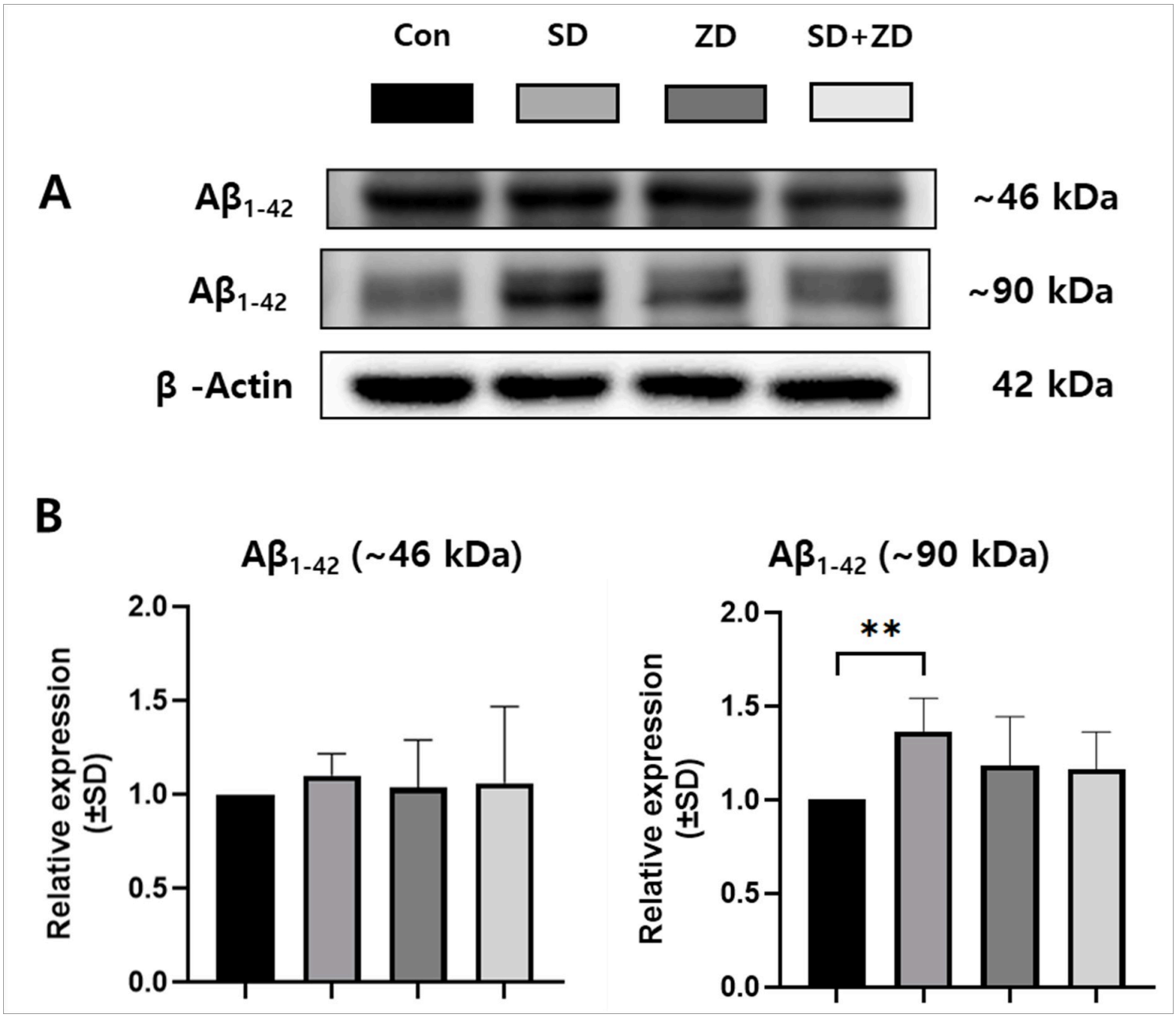


Figure 5

$A\beta_{1-42}$ immunoreactive species in brain parenchyma (BP). Western blot analysis of $A\beta_{1-42}$ immunoreactive bands at ~46 and ~90 kDa. Relative expression was normalized to β-actin. ($^{*}p < 0.05$, $^{**}p < 0.01$).

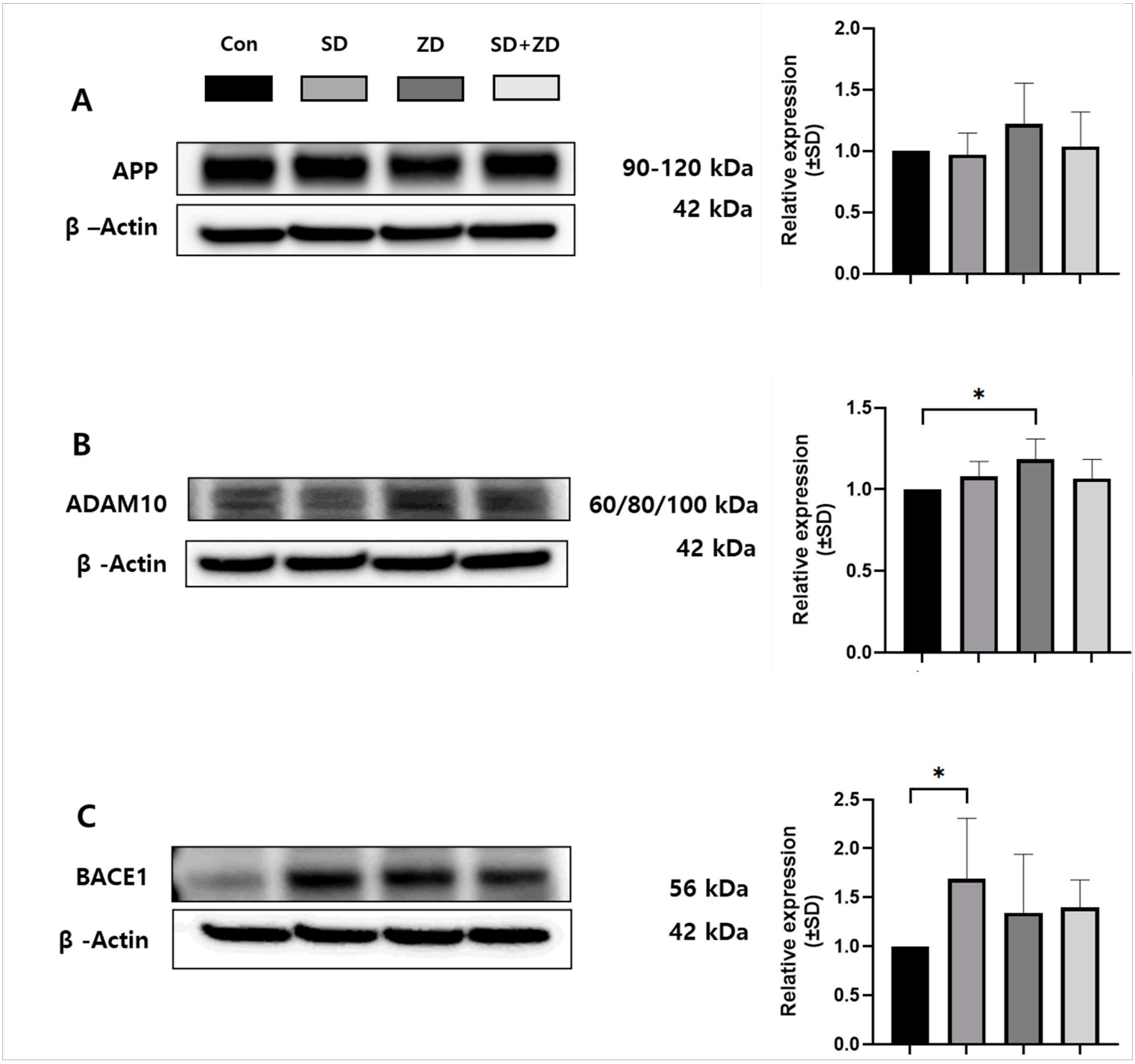


Figure 6

Amyloid precursor and processing proteins in brain parenchyma (BP). Western blot analysis of APP (90-120 kDa), BACE1 (56 kDa), and ADAM10 (60/80/100 kDa) in brain parenchyma. Relative expression normalized to β-actin ($^{*}p < 0.05$).

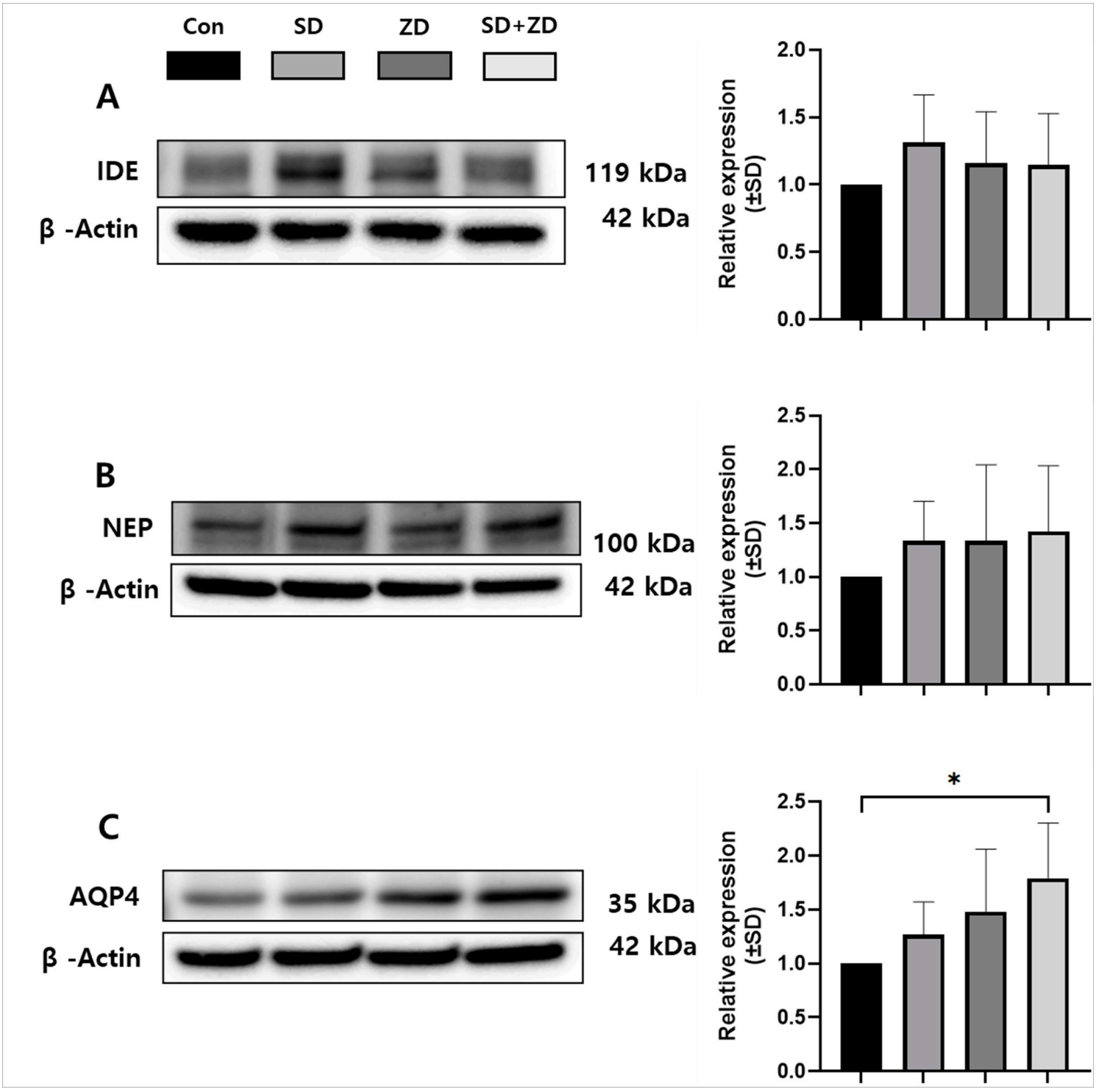


Figure 7

Aβ-degrading enzymes in brain parenchyma (BP). Protein levels of IDE, NEP and AQP4 in brain parenchyma. ($^{*}p < 0.05$).

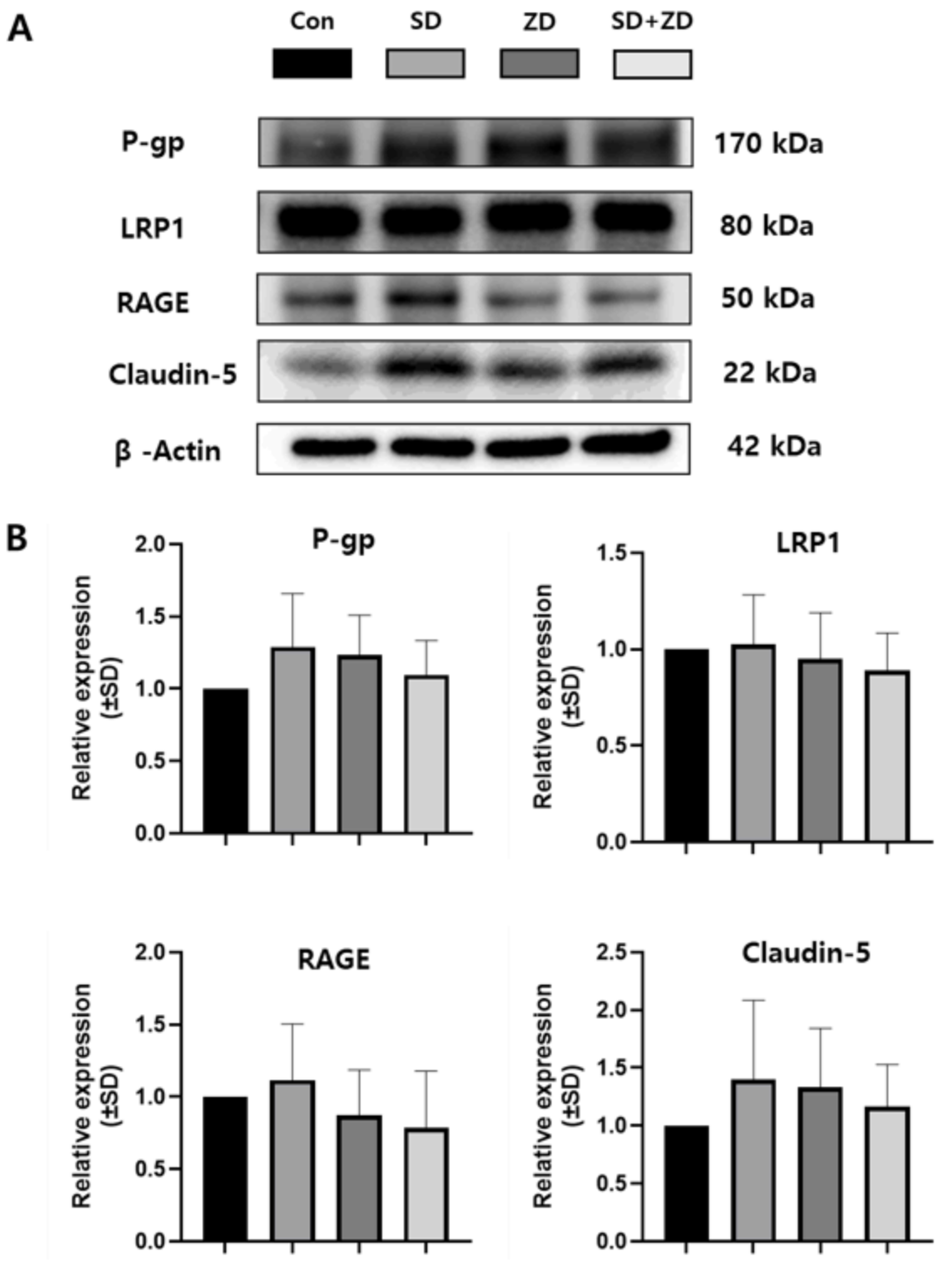


Figure 8

Aβ transporters and tight junction proteins. Western blot of P-gp, RAGE, LRP1, and claudin-5 in BCE and in BP fractions.

Supplementary Files

This is a list of supplementary files associated with this preprint. Click to download.

- AntibodyBP.pptx
- Antibody20251030BCE.pptx
- Supplement.docx